Magnetic Resonance in Medicine 57:249–257 (2007)

Sensitivity-Encoded (SENSE) Proton Echo-Planar Spectroscopic Imaging (PEPSI) in the Human Brain

Fa-Hsuan Lin,[1,2*] Shang-Yueh Tsai,[1,3] Ricardo Otazo,[4,5] Arvind Caprihan,[4,6] Lawrence L. Wald,[1,2] John W. Belliveau,[1,2] and Stefan Posse[4,5,7]

Magnetic resonance spectroscopic imaging (MRSI) provides spatially resolved metabolite information that is invaluable for both neuroscience studies and clinical applications. However, lengthy data acquisition times, which are a result of time-consuming phase encoding, represent a major challenge for MRSI. Fast MRSI pulse sequences that use echo-planar readout gradients, such as proton echo-planar spectroscopic imaging (PEPSI), are capable of fast spectral-spatial encoding and thus enable acceleration of image acquisition times. Combining PEPSI with recent advances in parallel MRI utilizing RF coil arrays can further accelerate MRSI data acquisition. Here we investigate the feasibility of ultrafast spectroscopic imaging at high field (3T and 4T) by combining PEPSI with sensitivity-encoded (SENSE) MRI using eight-channel head coil arrays. We show that the acquisition of single-average SENSE-PEPSI data at a short TE (15 ms) can be accelerated to 32 s or less, depending on the field strength, to obtain metabolic images of choline (Cho), creatine (Cre), N-acetyl-aspartate (NAA), and J-coupled metabolites (e.g., glutamate (Glu) and inositol (Ino)) with acceptable spectral quality and localization. The experimentally measured reductions in signal-to-noise ratio (SNR) and Cramer-Rao lower bounds (CRLBs) of metabolite resonances were well explained by both the *g*-factor and reduced measurement times. Thus, this technology is a promising means of reducing the scan times of 3D acquisitions and time-resolved 2D measurements. Magn Reson Med 57:249–257, 2007. © 2007 Wiley-Liss, Inc.

Key words: SENSE; PEPSI; parallel MRI; spectroscopic imaging; MRS

Magnetic resonance spectroscopic imaging (MRSI) measures spatially encoded time-domain signals from free induction decay (FID), stimulated echoes, or spin echoes to resolve the 2D or 3D spatial distribution of spectroscopic information originating from different locations within the field of view (FOV) (1–5). The data acquisition time of MRSI grows in proportion to the spatial encoding specified in the imaging protocol. For example, the encoding time for 2D proton MRSI with a 32×32 imaging matrix and TR of 2 s is more than 30 min. Reduced *k*-space encoding schemes can considerably reduce acquisition times in clinical studies (6), but 3D spatial encoding is still not feasible within clinically acceptable measurement times. The quality of data acquired during such lengthy acquisition times can be seriously degraded as a result of either head motion or scanner instability. Furthermore, dynamic metabolic imaging, which requires repeated measurements to obtain time-resolved information, is limited to rather coarse temporal resolution.

One method of reducing the data acquisition time of MRSI is to acquire multiple individually phase-encoded spin echoes in a single RF excitation (7). Much faster spatial-spectral encoding can be achieved using either echo-planar imaging (EPI) (8) or spiral readouts (9). Proton echo-planar spectroscopic imaging (PEPSI) uses echo-planar readouts to accelerate spatial encoding times by more than one order of magnitude, and was developed for clinical MR scanners to measure 2D metabolite distributions at short TE and 3D metabolite distributions (10,11). PEPSI has also been employed for time-resolved metabolic imaging to dynamically map lactate (Lac) concentrations during respiratory and metabolic challenges (11,12) and to characterize metabolic dysfunction during sodium-Lac infusion in patients with panic disorder (13).

Recent advances in parallel MRI, which employs information from different channels in an RF coil array, can further accelerate data acquisition. In parallel MRI, spatial encoding time is shortened by sparse *k*-space sampling. Because it fails to satisfy the Nyquist sampling criterion, direct Fourier reconstruction of parallel MRI data results in aliased images. Such aliased images from multiple RF channels can be combined to reconstruct full-FOV images without aliasing. Different parallel MRI reconstruction methods, including image-domain sensitivity encoding (SENSE) (14) and *k*-space-domain simultaneous acquisition of spatial harmonics (SMASH) (15), have also been proposed to reconstruct full-FOV images from parallel MRI acquisitions. The reduced encoding time for parallel MRI can be exchanged for higher spatiotemporal resolution (16–20); however, as with all fast-imaging techniques, including PEPSI, the cost of the above-mentioned benefits is a reduced signal-to-noise ratio (SNR) in the reconstructed image compared to the unaccelerated data. There are two reasons for SNR degradation in the reconstructed

[1]MGH-HMS-MIT Athinoula A. Martinos Center for Biomedical Imaging, Charlestown, Massachusetts, USA.

[2]Department of Radiology, Massachusetts General Hospital, Boston, Massachusetts, USA.

[3]Department of Electrical Engineering, National Taiwan University, Taipei, Taiwan.

[4]MIND Institute, Albuquerque, New Mexico, USA.

[5]Electrical and Computer Engineering Department, University of New Mexico, Albuquerque, New Mexico, USA.

[6]New Mexico Resonance, Albuquerque, New Mexico, USA.

[7]Department of Psychiatry, University of New Mexico, Albuquerque, New Mexico, USA.

Grant sponsor: National Institutes of Health (NIH); Grant numbers: R01 HD040712; R01 NS037462; R01 EB000790-04; P41 RR14075; R01 DA14178-01; Grant sponsor: Mental Illness and Neuroscience Discovery Institute (MIND).

Presented in part at the 13th Annual Meeting of ISMRM, Miami Beach, FL, USA, 2005.

*Correspondence to: Fa-Hsuan Lin, Ph.D., Athinoula A. Martinos Center for Biomedical Imaging, Bldg. 149, 13th Street, Mail Code 149-2301, Charlestown, MA 02129. E-mail: fhlin@nmr.mgh.harvard.edu

Received 3 October 2005; revised 15 September 2006; accepted 19 September 2006.

DOI 10.1002/mrm.21119
Published online in Wiley InterScience (www.interscience.wiley.com).

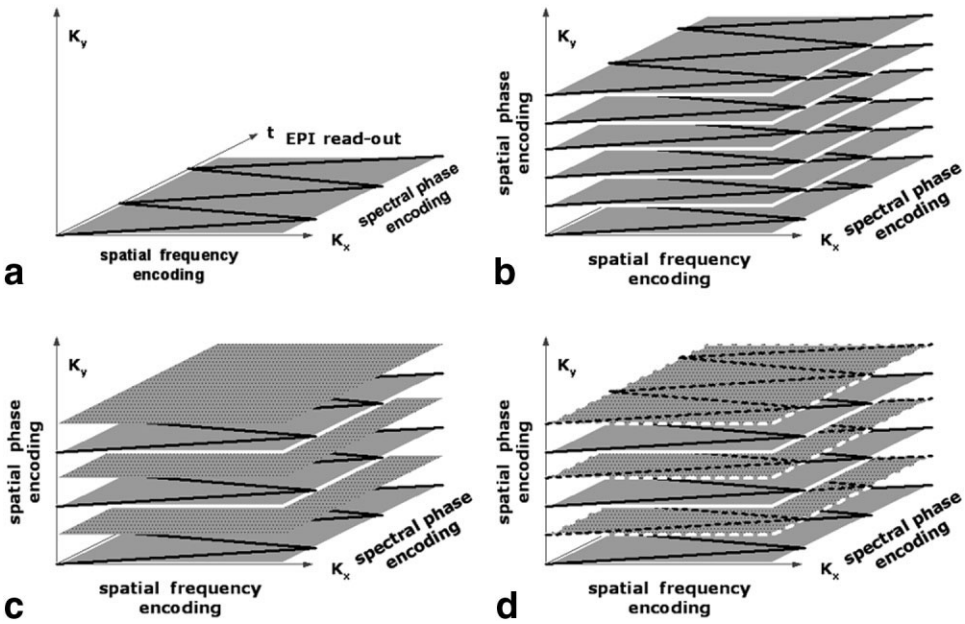

FIG. 1. Schematic diagram of SENSE-PEPSI data acquisition. **a:** PEPSI uses EPI for fast spatial-spectral encoding (white solid lines). **b:** For 2D spectroscopic imaging in PEPSI, spatial phase encoding is used to localize spectral information in conjunction with EPI-based spatiospectral encoding. **c:** SENSE involves skipping spatial phase-encoding steps to yield aliasing. Here we illustrate the 2X acceleration. **d:** Skipped data in SENSE PEPSI acquisition are interpolated using SENSE reconstruction (white dashed lines).

images: 1) parallel MRI acquires fewer data samples, and 2) ill conditioning of the encoding matrix increases the instability of parallel MRI reconstruction. The combination of these two major sources of SNR deterioration has been analyzed quantitatively (14). Methods to mitigate these problems include using variable-density sampling to emphasize the center of the *k*-space (21), employing prior information by regularizing the encoding matrix (22), and using coil array designs dedicated for parallel imaging (23,24).

In this study we combined PEPSI and parallel MRI (specifically SENSE reconstructions) to further accelerate the data acquisition for high-speed, single-average spectroscopic imaging (SENSE-PEPSI). With this combined method, SNR is traded for rapid spatial encoding. For this proof-of-concept study we used an eight-channel head coil array to characterize spectral quality and SNR at high fields (3T and 4T). We present both simulation results and experimentally acquired accelerated data in the sections that follow, and discuss the advantages and limitations of this MRSI data acquisition protocol.

MATERIALS AND METHODS

Data Acquisition

Human subjects were recruited for the present experiments with their informed consent and under the supervision of the Massachusetts General Hospital Institutional Review Board. We performed PEPSI (10) on healthy volunteers, using 3T (Trio; Siemens Medical Solution, Erlangen, Germany) and 4T (MedSpec; Bruker BioSpin MRI, Ettlingen, Germany) MR scanners equipped with eight-channel surface coil arrays that covered the entire head circumferentially with eight surface coils. PEPSI is a fast MRSI technique that includes water suppression by chemical shift selective saturation (CHESS) (25) using the water suppression enhanced through T_1 effects (WET) technique, eight slices of outer volume lipid suppression applied along the perimeter of the brain, spin-echo excitation, and fast spatial-spectral encoding of half-echoes using an EPI readout gradient train along the *x*-axis (10). We acquired data at 83.33 kHz, with 1024 gradient inversions and online regridding to account for ramp sampling. After the even-odd echoes were separated, the spectral bandwidth was 1087 Hz (26). We applied additional phase encoding along the *y*-axis to obtain 2D spatial encoding. To employ SENSE for spatiotemporal acceleration, we reduced the sampling of phase-encoding steps along the *y*-axis by sampling one *k*-space line in a block of two, three, or four consecutive *k*-space lines in the phase-encoding direction, in order to achieve accelerations of 2X, 3X, and 4X, respectively. Figure 1 shows a schematic representation of the PEPSI sequence and the SENSE-PEPSI acquisition. The acquisition protocol included both water-suppressed (WS) and non-WS (NWS) scans. NWS data were collected without spatial presaturation and were used for automatic phase and frequency shift correction.

We acquired fully sampled and SENSE-accelerated single-average in vivo PEPSI data from a para-axial slice at the upper edge of the ventricles (TR = 2 s, TE = 15 ms, 32 × 32 spatial matrix, FOV = 220 mm). The data acquisition time was 64 s without SENSE acceleration. The acquisition times for accelerated in vivo data acquired with 2X, 3X, and 4X SENSE along the anterior–posterior direction were 32, 22, and 16 s, respectively. A 3T phantom data set with full phase encoding was collected using a spherical spectroscopic phantom containing a mixture of metabolite solutions, including choline (Cho), creatine (Cre), N-acetyl-aspartate (NAA), inositol (Ino), glutamate (Glu), glutamine (Gln), and Lac. To investigate degradation of SNR without the presence of additional complicating factors, such as changes in frequency drift resulting from gradient heating, we reduced the fully sampled *k*-space

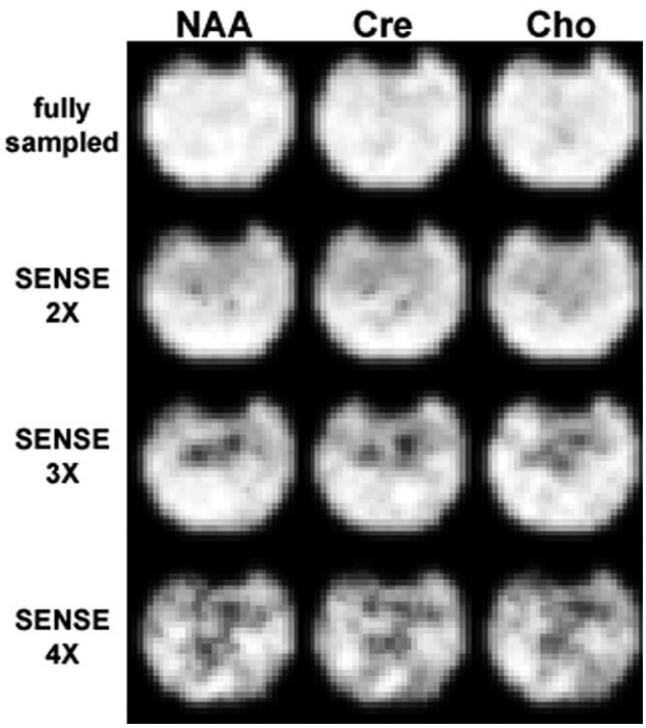

FIG. 2. WS metabolite maps using LCModel quantification from fully sampled PEPSI data, and 2X, 3X, and 4X SENSE accelerated scans. The metabolites include NAA, Cre, and Cho.

data along the phase-encoding direction to simulate acceleration rates of 2X, 3X, and 4X.

SENSE Reconstruction

Each PEPSI scan was separated into even- and odd-echo data, which were processed separately. We applied a sinusoidal *k*-space filter to both NWS and WS data to suppress side lobes of the point-spread function (PSF). To reconstruct SENSE-accelerated data, one must first obtain coil sensitivity maps. Because PEPSI requires NWS reference data for automatic phasing, frequency shift, and eddy-current corrections, we used the water spectral images in the NWS reference data without SENSE acceleration to estimate coil sensitivity maps. Based on our previous experience in reconstructing SENSE EPI data (27), we further fit the water spectral images with a third-order polynomial to remove potential anatomical features inside the low-resolution NWS water spectral images. We implemented a standard SENSE reconstruction algorithm (14) to unfold the individual aliased spectral images in the anterior–posterior direction at 2X, 3X, and 4X accelerations. In addition to requiring accelerated SENSE data and coil sensitivity maps, SENSE reconstruction also depends on a noise covariance matrix. We characterized this matrix by measuring the complex-valued data from each channel of the array after switching off the spatial-encoding gradients and RF excitation. The time series measurements from each channel of the RF coil were concatenated to form an *m*-by-*t* matrix **Y**, where *m* is the number of the RF receiver in the array, and *t* is the number of data samples in each time series. The noise covariance matrix Φ was calculated as $\Phi = \langle (Y - \overline{Y})(Y - \overline{Y})^H \rangle$, where $\langle \bullet \rangle$ denotes the average over time, $\overline{Y}$ denotes the average of Y, and the superscript *H* denotes the complex conjugate and transpose.

Given the concatenated accelerated measurements, $\overline{y}$, an encoding matrix, E, and a noise covariance matrix, Φ, weighted least-squares fitting leads to the solution of the reconstructed full-FOV image, $\overline{x}$ (14):

$$\overline{x} = (E^H \Phi^{-1} E)^{-1} E^H \Phi^{-1} \overline{y}, \quad [1]$$

where E is the combination of the coil sensitivity maps, *k*-space sampling, and the discrete-time Fourier transform. We evaluated the quantification of local noise amplification in the SENSE reconstruction due to conditioning of the encoding matrix using the *g*-factor (14), i.e., the ratio of the noise levels between the accelerated reconstruction and the unaccelerated reconstruction normalized by the square root of the acceleration factor:

$$g_{\rho\rho} = \sqrt{[(E^H \Phi^{-1} E)^{-1}]_{\rho\rho} [(E^H \Phi^{-1} E)]_{\rho\rho}} \quad [2]$$

where the subscript ρ represents the spatial index to a pixel. The SNR ratio between *R*-fold accelerated and unaccelerated at a reconstructed pixel is thus derived:

$$\frac{SNR_{\rho}^{un\text{-}accelerated}}{SNR_{\rho}^{accelerated}} = \sqrt{R} \cdot g_{\rho\rho} \quad [3]$$

Postprocessing of the Reconstructed Spectra and Error Quantification

After SENSE reconstruction of the WS data, at each spectral point, we performed a pixelwise multiplication of unaliased magnetization map and individual coil maps used in the SENSE reconstruction to obtain multiple unaliased images with coil sensitivity modulation. This is

Table 1
3T Phantom Experiment: SNR, Relative SNR in SENSE Accelerated Scan with Respect to Fully-Sampled Data, and Predicted SNR Degradation Using g-Factor and SENSE Acceleration Rates for NAA, Creatine (Cre), and Choline (Cho) Metabolite Ranges*

	Fully-sampled SNR	SENSE 2X		SENSE 3X		SENSE 4X	
		SNR	rSNR	SNR	rSNR	SNR	rSNR
NAA	20.07	14.11	1.42	7.52	2.67	1.90	10.54
Cre	17.21	9.43	1.82	5.09	3.38	2.28	7.56
Cho	21.87	12.37	1.77	8.13	2.69	2.07	10.59

*The theoretical SNR degradation quantified by $\overline{g}\sqrt{R}$ is 1.70, 3.12, and 8.92, for 2X, 3X, and 4X SENSE, respectively.

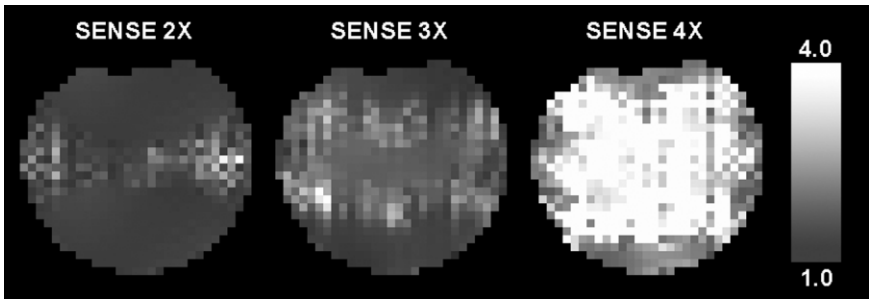

FIG. 3. *g*-Factor maps from 2X, 3X, and 4X SENSE accelerations.

because we need to use the fully phase-encoded NWS scans from individual channels of the array for subsequent automatic phasing (28), frequency shift, and eddy-current corrections. This step provides coil-specific reconstructed WS spectral images that match the NWS data from individual channels of the coil array for subsequent postprocessing. We applied automatic zero-order phase correction to the SENSE-reconstructed even and odd data separately. We then combined both echoes separately for each coil and applied eddy-current correction based on the NWS scan. Finally, we averaged all channels to produce spectroscopic images (28).

We summarized the performance of the phantom SENSE-PEPSI reconstructions by a *g*-factor map to show the spatial distribution of noise amplification due to conditioning of the encoding matrix in the SENSE acquisition. We calculated both the averages and standard deviations (SDs) of the *g*-factors at each SENSE acceleration rate. Subsequently, we evaluated the SNR of the reconstructed spectra before we performed LCModel spectral fitting. We calculated the signal of a metabolite peak as the integral of the absolute value of the data over 0.1 ppm (symmetric around the metabolite maximum), and then used the SD of the real part of the spectrum between 7.5 ppm and 8.5 ppm to estimate the noise of a metabolite from the 3T phantom experiment. This procedure corresponds to the following equation for SNR estimation:

$$SNR = \frac{\left\langle \sum_{j\in SIGNAL} |d_j| / n_{signal} \right\rangle}{\left\langle \sqrt{\sum_{i\in NOISE} \mathrm{Re}(d_i)^2 / n_{noise}} \right\rangle} \quad [4]$$

where n_{signal} and n_{noise} represent the numbers of spectral points in the metabolite and noise range, respectively; d_j indicates the reconstructed spectrum with spectral index j; and $\langle\bullet\rangle$ represents the spatial average across the FOV. We calculated the SNR relative to the full sampled data as:

$$rSNR = \frac{SNR_{full\ sampled}}{SNR_{accelerated}}. \quad [5]$$

In theory, we expect good agreement between *rSNR* and a theoretical prediction $\bar{g}\sqrt{R}$, where $\bar{g}$ is the spatial average of the *g*-factor, and *R* denotes the SENSE acceleration rate.

For the in vivo data, we employed LCModel fitting (29) for absolute quantification using the water-scaling method (29). The LCModel fitting also included simulated macromolecules and lipid components. The spectral fitting range was between 0.2 and 4 ppm. The Cramer-Rao lower bound (CRLB, the lowest bound of the SD of the estimated metabolite concentration expressed as percentage of concentration) is commonly used to quantify the goodness-of-fit of LCModel outputs. We used the following thresholds to

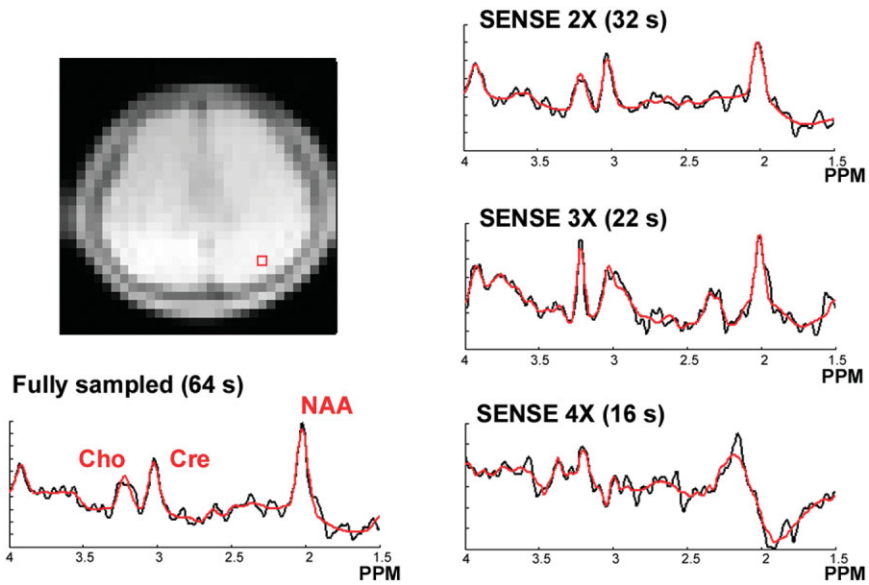

FIG. 4. A representative single-average 3T spectrum from fully sampled PEPSI data with an acquisition time of 64 s, as well as from 2X, 3X, and 4X SENSE accelerations with data acquisition times of 32, 22, and 16 s, respectively. The location of the voxel is indicated by the red box on a NWS image. The red box in the figure indicates the location of the selected voxel. The black broken line and red solid line spectra represent measured and LCModel fitted spectra, respectively.

reject spectroscopic image voxels with unsatisfactory LCModel fit results: 1) CRLB $< 30\%$ for NAA and Cr, and CRLB $< 50\%$ for Cho, Glu, and Ino, and 2) spectral linewidth < 0.1 ppm. We excluded above-threshold voxels from the metabolite maps. We quantified the overall goodness-of-spectra-fit by calculating the average CRLB across all subthreshold voxels within the brain.

In this study, we reported all NAA, Cre, and Cho concentration values in millimolar (mM) units. The metabolite concentrations were not corrected for relaxation time in this study and thus they may appear on the high end. We used the same mM units to express the difference between metabolite-concentration images of SENSE reconstructed data and fully phase-encoded data in order to quantify the quality of SENSE reconstructions. Finally, we interpolated the metabolite maps to obtain 128×128 images for visualization.

RESULTS

Single Average 3T Phantom Study

Figure 2 shows the single-average fully sampled and 2X, 3X, and 4X SENSE-accelerated PEPSI WS reconstructed images from a spectral phantom at 3T. The reconstructed 2X image shows homogeneous metabolite concentrations in the periphery, with inhomogeneity at the center of the FOV. The 3X-accelerated image shows slight inhomogeneity across the FOV, with large spatial noise at the center of the FOV. The 4X-accelerated image is noisy and shows considerable reconstruction artifact compared to the unaccelerated data. In general, we observed degradation of the metabolite image quality with an increasing SENSE acceleration rate. When we quantified SNR at 2X, 3X, and 4X accelerations, we found that it degraded monotonically in accordance with the increased acceleration rate. These results are reported in Table 1.

An examination of the *g*-factor maps reveals the spatial distribution of noise amplification derived from the unfolding process in SENSE reconstruction. Figure 3 shows the *g*-factor maps of 2X, 3X, and 4X SENSE reconstructions using coil sensitivity profiles estimated from the water spectral images of NWS scans. Because identical estimated coil sensitivity profiles were utilized for SENSE reconstruction, the *g*-factors remained invariant across metabolites. As expected, higher *g*-factors were found at the center of the FOV for the 2X SENSE acceleration, in agreement with the finding in WS-reconstructed metabolite images shown in Fig. 2. 3X SENSE showed three horizontal bands corresponding to the expected unfolding noise amplification from 3X-accelerated data. 4X SENSE reconstructions showed higher *g*-factors across the FOV than either the 2X and 3X accelerated images. Quantitatively, the averaged *g*-factors at 2X, 3X, and 4X were 1.22 ± 0.28, 1.85 ± 0.42, and 4.46 ± 0.93, respectively. By cross-validating the SNRs reported in Table 1, we found good agreement between the theoretical prediction ($(\bar{g}\sqrt{R})$) and the measured relative SNR (rSNR).

Single-Average Human 3T Study

Figure 4 shows the reconstructed spectra of a representative voxel after LCModel fitting was performed on the single-average PEPSI data. WS data were acquired in 64, 32, 22, and 16 s for fully sampled, 2X, 3X, and 4X SENSE accelerations, respectively. We also observed three major metabolite peaks with similar widths and shapes in the fully sampled and 2X-accelerated data. Note that because both 3X and 4X data exhibited increased noise levels, it was difficult to identify Cre and Cho peaks. The shapes of the baselines in all reconstructed data were of similar quality and did not exhibit significant unfolding artifacts.

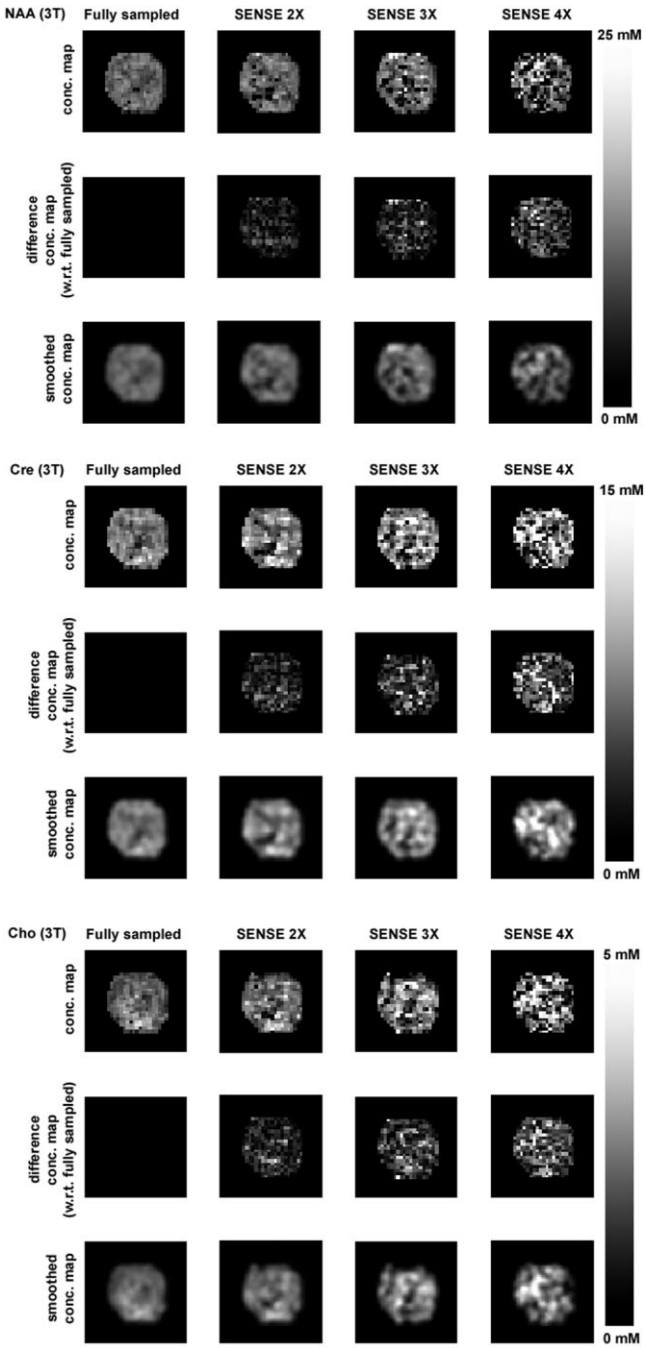

FIG. 5. 3T LCModel-quantified metabolite concentration maps, difference metabolite concentration maps with respect to fully sampled PEPSI data, and spatially smoothed concentration maps for NAA, Cre, and Cho from fully sampled PEPSI data and 2X, 3X, and 4X SENSE accelerations.

Table 2
Averages and SDs of Metabolite Concentrations (in mM) in Fully Sampled Data and 2X, 3X, and 4X SENSE Accelerations at 3T and 4T

	Fully sampled	SENSE 2X	SENSE 3X	SENSE 4X
3T				
NAA	16.58 ± 7.21	16.76 ± 7.64	17.2 ± 7.87	18.39 ± 7.34
Cre	12.60 ± 6.11	13.51 ± 6.62	13.59 ± 7.04	17.29 ± 7.71
Cho	2.99 ± 1.52	3.17 ± 1.56	4.08 ± 1.82	5.14 ± 1.91
4T				
NAA	17.25 ± 6.9	17.67 ± 7.1	18.66 ± 6.9	19.24 ± 5.9
Cre	13.47 ± 5.3	13.11 ± 5.2	14.32 ± 5.3	16.21 ± 4.6
Cho	3.26 ± 1.3	3.15 ± 1.3	3.48 ± 1.3	4.34 ± 1.1

3T in vivo Cho, Cre, and NAA metabolite maps are shown in Fig. 5. The average metabolite concentrations (with SDs) for different acceleration factors are listed in Table 2. The metabolite concentrations increased slightly as the acceleration factor increased. To compare the fully sampled data and SENSE reconstructions, we also show difference metabolite maps using the same scale (Fig. 5). NAA, Cho, and Cre metabolite images using SENSE 2X reconstruction were similar to those obtained with fully sampled data, as quantified by the difference concentration maps. The root-mean-square (RMS) concentration differences between 2X SENSE and fully sampled data for NAA, Cre, and Cho were 3.54 mM, 3.16 mM, and 1.14 mM, respectively (Table 3). Qualitatively, the 3X and 4X SENSE results failed to preserve the homogenous metabolite distribution in brain parenchyma regions seen in the fully sampled and 2X SENSE data. We quantified the goodness of the LCModel fit by computing the averages of the CRLBs across the imaging slice (Table 4). Both the fully sampled data and the 2X SENSE reconstructions had CRLBs of less than 15% for NAA and Cre.

Single-Average Human 4T Study

Fully sampled and 2X, 3X, and 4X SENSE-accelerated PEPSI data were acquired with a single signal average. Figure 6 shows representative reconstructed spectra in the parietal lobe parenchyma. The major metabolite peaks, including NAA, Cre, and Cho, in the fully sampled and 2X and 3X SENSE-accelerated data were well resolved. At 4X acceleration, the data were noisy, and the Cre and Cho metabolite peaks were difficult to distinguish from background noise. Reconstructed metabolite maps are shown in Fig. 7, and the corresponding metabolite concentration values are shown in Table 2. We found consistent results when we compared the fully sampled data with the 2X SENSE reconstruction. Qualitatively, we observed homogeneous metabolite concentrations in the parenchyma and reduced metabolite concentration in the central ventricular regions of both data sets. Quantitatively, the differences in RMS concentration between the fully sampled data and the 2X SENSE data were 1.98 mM, 1.70 mM, and 0.87 mM for NAA, Cre, and Cho, respectively (Table 3). Larger differences in RMS metabolite concentrations were reported for 3X and 4X SENSE reconstructions, as shown in Table 3. Metabolite maps acquired with 3X acceleration showed increased inhomogeneity of the spatial metabolite distribution, which degraded even more at 4X SENSE acceleration. The CRLBs of all metabolite maps are summarized in Table 4. We found that for both NAA and Cre, fully sampled and 2X SENSE data had CRLBs of less than 10%. Overall, compared to 3T, the higher intrinsic SNR at 4T enabled us to achieve higher-quality metabolite maps with 2X and 3X acceleration. Figure 8 shows the glutamate (Glu) and inositol (Ino) metabolite maps after LCModel quantification with full phase encoding and 2X, 3X, and 4X SENSE accelerations. The 2X SENSE and fully sampled data were similar. The average concentrations of Glu for the fully sampled and 2X SENSE data were 17.9 mM and 17.8 mM, respectively, while those of Ino were 10.6 mM and 10.4 mM for fully sampled and 2X SENSE data, respectively.

DISCUSSION

In this paper we demonstrate the feasibility of using SENSE reconstruction to accelerate single-average, high-

Table 3
Root-Mean-Square (RMS) of the Difference in Metabolite Concentrations (in mM) Between Fully Sampled Data and SENSE Reconstructions of NAA, Creatine (CRE), and Choline (Cho) at 3T and 4T

	Fully sampled	SENSE 2X	SENSE 3X	SENSE 4X
3T				
NAA	N/A	3.54	6.96	10.32
Cre	N/A	3.16	6.39	8.86
Cho	N/A	1.14	2.37	2.81
4T				
NAA	N/A	1.98	6.71	12.27
Cre	N/A	1.70	5.55	9.76
Cho	N/A	0.87	1.55	2.58

Table 4
Averages of Cramer-Rao-lower-bounds (CRLB) of NAA, Creatine (CRE), and Choline (Cho) in Fully-Sampled Data and 2X, 3X, and 4X SENSE Accelerations at 3T and 4T

	Fully-sampled	SENSE 2X	SENSE 3X	SENSE 4X
3T				
NAA	8.84	12.05	16.49	24.39
Cre	9.37	11.97	18.77	37.87
Cho	17.05	22.89	26.79	46.53
4T				
NAA	6.60	9.00	11.80	19.40
Cre	7.20	9.60	18.70	35.30
Cho	13.30	19.60	26.40	47.30

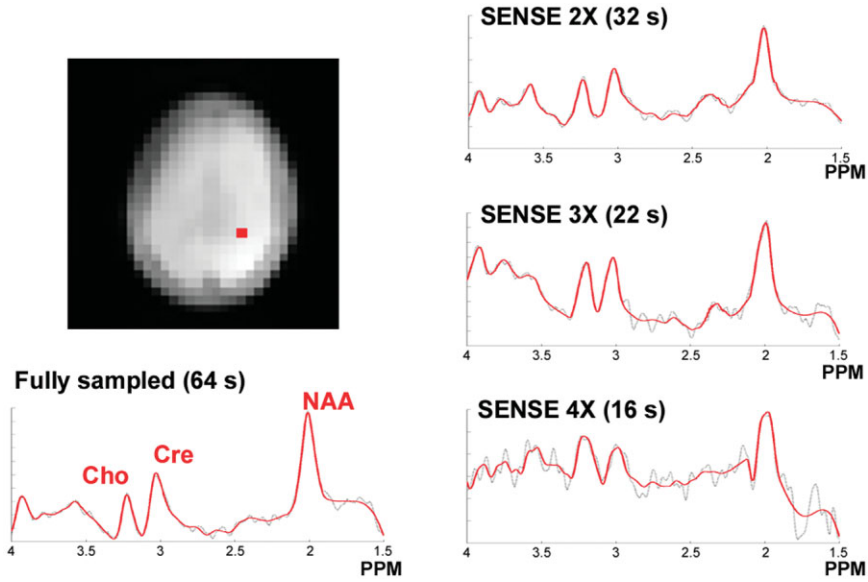

FIG. 6. A representative single-average 4T spectrum from fully sampled PEPSI data with an acquisition time of 64 s, and from 2X, 3X, and 4X SENSE accelerations with data acquisition times of 32, 22, and 16 s, respectively. The location of the voxel is indicated by the red box on a NWS image. The red box in the figure indicates the location of the selected voxel. The black dash line and red solid line spectra represent measured and LCModel fitted spectra, respectively.

speed, gradient-encoded MRSI data acquisition. This acceleration is achieved by trading off image SNR for data acquisition time. SNR is reduced as a result of reduced numbers of data samples and reconstruction-associated noise amplification. In this study we show that at high field (≥3T), the combination of PEPSI and SENSE can reduce the single-average data acquisition time for a 32 × 32 image matrix from 64 to 32 s (2X SENSE) while maintaining similar metabolite concentration values. With even higher field strength and improved RF coil arrays, we anticipate that SENSE-accelerated single-average metabolite mapping with scanning times on the order of a few seconds will become feasible. Single-average SENSE-PEPSI is particularly appealing for experiments with transient high SNR, such as those using hyperpolarized ^{13}C (30).

Our data at 1.5T (not included here) show that single-average SENSE-PEPSI is not feasible due to SNR limitations at lower field, in which case averaging is necessary to obtain sufficient SNR. Thus, at lower fields, the advantage of SENSE-PEPSI may be primarily the reduction of intrascan motion sensitivity due to shortened acquisition times for each measurement average. However, the possible benefits of reduced motion sensitivity with acceleration remain to be defined by further experimental investigations.

Previous studies of MRSI combined with parallel MRI used either conventional chemical-shift imaging (CSI) encoding (31) or multiple spin-echo acquisitions (32). These methods have been shown to accelerate imaging acquisition time from 22.5 min to 5.5 min (at 4X acceleration, TR = 1.5 s) or 2.5 min (at 4X acceleration and four echoes, TR = 1.5 s) for experiments with an image matrix size of 32 × 32. However, the cost of acceleration was degraded SNR resulting from the combination of the *g*-factor and data samples/scan time. In these studies, acceleration was performed in two spatial dimensions, and the results thus correspond to our results using 2X acceleration along the phase-encoding direction. Acceleration along a second in-plane spatial dimension is not feasible using PEPSI, since 2D PEPSI has only one phase-encoding dimension and therefore cannot be further accelerated by SENSE.

SENSE acceleration is particularly important for reducing long scan times in 3D spatial encoding. As mentioned above, 1D SENSE acceleration can be utilized to accelerate the slow spatial phase encoding in a 2D PEPSI experiment. One can achieve further acceleration by employing 2D SENSE in 3D PEPSI experiments that use two orthogonal spatial phase-encoding gradients. The SENSE-PEPSI imaging technique can also be generalized to other echo-planar-based readout methods, such as echo-shifted EPI (33) or spiral (9) MRSI. In these methods, oscillating readout gradients are used to encode 2D spatial information in a single shot, which makes direct application of 2D SENSE application feasible. In fact, the cylindrically symmetric layout of the head RF array coil currently available encourages the use of 2D SENSE to minimize the *g*-factor (23,24). In other words, one can implement *R*-fold SENSE acceleration more efficiently by accelerating $R_x = R_y = \sqrt{R}$ in two orthogonal dimensions. In SENSE-PEPSI, this implies that the readout direction should be along the superior–inferior direction, with two orthogonal phase- and partition-encoding directions along the left–right and anterior–posterior directions.

The image reconstruction method reported here was adopted from the conventional SENSE method, although we used NWS data to estimate the coil sensitivity profile. NWS data are indispensable for subsequent data processing, such as phase correction, eddy-current correction, and B_0 shift correction, and thus the image acquisition time penalty is minor. One potential challenge posed by the use of NWS data for coil sensitivity map estimation is residual lipid contamination. Scalp lipid signals originate from peripheral regions outside the brain parenchyma that are close to the coil surface and contribute high MR signal intensity. The implication is that the estimated coil sensitivity profile derived from the NWS data set may be inaccurate in the vicinity of the scalp lipid region, and as a consequence SENSE reconstruction of metabolic images in the spectral range of lipids (e.g., Lac) may fail to remove aliasing. By extending the estimated coil sensitivity profiles by several voxels, one can improve the reconstruction

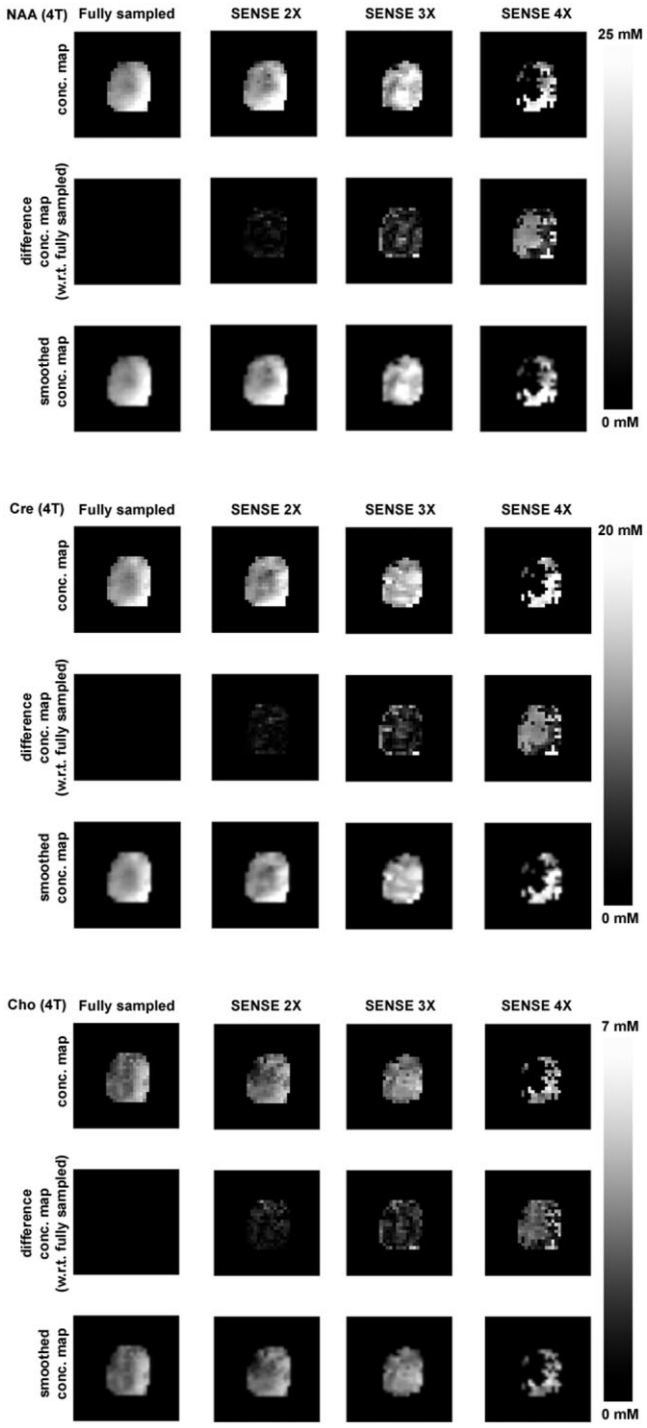

FIG. 7. 4T LCModel-quantified metabolite concentration maps, difference metabolite concentration maps with respect to fully sampled PEPSI data, and spatially smoothed concentration maps for NAA, Cre, and Cho from fully sampled PEPSI data and 2X, 3X, and 4X SENSE accelerations.

considerably (31). The same technique can be used to improve coil sensitivity maps for better image reconstruction at lipid frequencies. In this study we acquired fully sampled NWS data in each experiment. An alternative image reconstruction method is generalized autocalibrating partially parallel acquisitions (GRAPPA) (34), which employs the fully sampled data around the center of the *k*-space as autocalibration lines to estimate reconstruction coefficients.

In this study we used an eight-channel array coil for SENSE acceleration to yield satisfactory 2X accelerated reconstruction. We expect that successful acceleration of SENSE reconstruction depends on the geometry and the number of channels in the array coil. We also recently developed a large-*N* array coil with up to 32 channels for imaging the brain at 3T (35). The use of such array coils has the potential to increase the SENSE acceleration rate by fourfold without significant *g*-factor-related SNR degradation.

In future work we will further investigate the possibility of incorporating spectral priors to stabilize SENSE reconstruction. It has been shown that incorporating spatial priors can improve SENSE reconstructions in anatomical (22) and functional brain imaging (27). Given the range of metabolite concentrations in the normal human brain, we expect that the use of such prior information and an appropriate regularization parameters will further reduce the noise level of SENSE reconstruction.

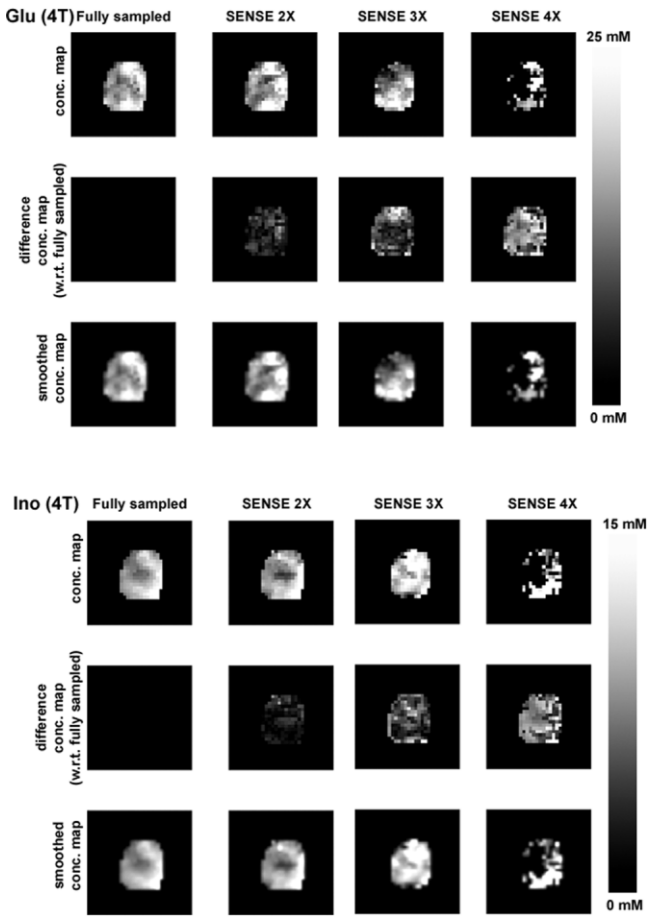

FIG. 8. 4T LCModel-quantified metabolite concentration maps, difference metabolite concentration maps with respect to fully sampled PEPSI data, and spatially smoothed concentration maps for Glu and Ino from fully sampled PEPSI data and 2X, 3X, and 4X SENSE accelerations.

CONCLUSIONS

In this work, we have presented the SENSE-PEPSI method, which can achieve accelerated, noninvasive, single-average measurements of metabolites in the human brain with high spatial-temporal resolution. We employed phantom studies using an eight-channel array coil to validate the SENSE-PEPSI technique. In vivo results at 3T and 4T demonstrate that single-average 2X SENSE-PEPSI, acquired in 32 s at a TR of 2 s for a 32 × 32 image matrix, provides metabolite images in good agreement with fully sampled data. SENSE-PEPSI may be used for fast, dynamic characterization of metabolism in human functional systems.

REFERENCES

1. Posse S, Schuknecht B, Smith ME, van Zijl PC, Herschkowitz N, Moonen CT. Short echo time proton MR spectroscopic imaging. J Comput Assist Tomogr 1993;17:1–14.
2. Nelson SJ, Vigneron DB, Star-Lack J, Kurhanewicz J. High spatial resolution and speed in MRSI. NMR Biomed 1997;10:411–422.
3. Dydak U, Schar M. MR spectroscopy and spectroscopic imaging: comparing 3.0 T versus 1.5 T. Neuroimaging Clin N Am 2006;16:269–283, x.
4. Duyn JH, Gillen J, Sobering G, van Zijl PC, Moonen CT. Multisection proton MR spectroscopic imaging of the brain. Radiology 1993;188:277–282.
5. Brown TR, Kincaid BM, Ugurbil K. NMR chemical shift imaging in three dimensions. Proc Natl Acad Sci USA 1982;79:3523–3526.
6. Maudsley AA, Matson GB, Hugg JW, Weiner MW. Reduced phase encoding in spectroscopic imaging. Magn Reson Med 1994;31:645–651.
7. Duyn JH, Moonen CT. Fast proton spectroscopic imaging of human brain using multiple spin-echoes. Magn Reson Med 1993;30:409–414.
8. Mansfield P. Multi-planar image formation using NMR spin echos. J Physics 1977;C10:L55–L58.
9. Adalsteinsson E, Irarrazabal P, Topp S, Meyer C, Macovski A, Spielman DM. Volumetric spectroscopic imaging with spiral-based k-space trajectories. Magn Reson Med 1998;39:889–898.
10. Posse S, Tedeschi G, Risinger R, Ogg R, Le Bihan D. High speed 1H spectroscopic imaging in human brain by echo planar spatial-spectral encoding. Magn Reson Med 1995;33:34–40.
11. Posse S, Dager SR, Richards TL, Yuan C, Ogg R, Artru AA, Muller-Gartner HW, Hayes C. In vivo measurement of regional brain metabolic response to hyperventilation using magnetic resonance: proton echo planar spectroscopic imaging (PEPSI). Magn Reson Med 1997;37:858–865.
12. Dager SR, Layton ME, Strauss W, Richards TL, Heide A, Friedman SD, Artru AA, Hayes CE, Posse S. Human brain metabolic response to caffeine and the effects of tolerance. Am J Psychiatry 1999;156:229–237.
13. Dager SR, Friedman SD, Heide A, Layton ME, Richards T, Artru A, Strauss W, Hayes C, Posse S. Two-dimensional proton echo-planar spectroscopic imaging of brain metabolic changes during lactate-induced panic. Arch Gen Psychiatry 1999;56:70–77.
14. Pruessmann KP, Weiger M, Scheidegger MB, Boesiger P. SENSE: sensitivity encoding for fast MRI. Magn Reson Med 1999;42:952–962.
15. Sodickson DK, Manning WJ. Simultaneous acquisition of spatial harmonics (SMASH): fast imaging with radiofrequency coil arrays. Magn Reson Med 1997;38:591–603.
16. Bammer R, Auer M, Keeling SL, Augustin M, Stables LA, Prokesch RW, Stollberger R, Moseley ME, Fazekas F. Diffusion tensor imaging using single-shot SENSE-EPI. Magn Reson Med 2002;48:128–136.
17. Maki JH, Wilson GJ, Eubank WB, Hoogeveen RM. Utilizing SENSE to achieve lower station sub-millimeter isotropic resolution and minimal venous enhancement in peripheral MR angiography. J Magn Reson Imaging 2002;15:484–491.
18. Preibisch C, Pilatus U, Bunke J, Hoogenraad F, Zanella F, Lanfermann H. Functional MRI using sensitivity-encoded echo planar imaging (SENSE-EPI). Neuroimage 2003;19(2 Pt 1):412–421.
19. Jaermann T, Crelier G, Pruessmann KP, Golay X, Netsch T, van Muiswinkel AM, Mori S, van Zijl PC, Valavanis A, Kollias S, Boesiger P. SENSE-DTI at 3 T. Magn Reson Med 2004;51:230–236.
20. Summers PE, Kollias SS, Valavanis A. Resolution improvement in thick-slab magnetic resonance digital subtraction angiography using SENSE at 3T. J Magn Reson Imaging 2004;20:662–673.
21. Madore B. UNFOLD-SENSE: a parallel MRI method with self-calibration and artifact suppression. Magn Reson Med 2004;52:310–320.
22. Lin FH, Kwong KK, Belliveau JW, Wald LL. Parallel imaging reconstruction using automatic regularization. Magn Reson Med 2004;51:559–567.
23. de Zwart JA, Ledden PJ, Kellman P, van Gelderen P, Duyn JH. Design of a SENSE-optimized high-sensitivity MRI receive coil for brain imaging. Magn Reson Med 2002;47:1218–1227.
24. de Zwart JA, Ledden PJ, van Gelderen P, Bodurka J, Chu R, Duyn JH. Signal-to-noise ratio and parallel imaging performance of a 16-channel receive-only brain coil array at 3.0 Tesla. Magn Reson Med 2004;51:22–26.
25. Haase A, Frahm J, Hanicke W, Matthaei D. 1H NMR chemical shift selective (CHESS) imaging. Phys Med Biol 1985;30:341–344.
26. O'Sullivan J. A fast sinc function gridding algorithm for Fourier inversion in computer tomography. IEEE Trans Med Imaging 1985;MI–4:200–207.
27. Lin FH, Huang TY, Chen NK, Wang FN, Stufflebeam SM, Belliveau JW, Wald LL, Kwong KK. Functional MRI using regularized parallel imaging acquisition. Magn Reson Med 2005;54:343–353.
28. Posse S, Otazo R, Caprihan A, Xu J, Li T, Gasparovic C, Holten D, Alger JR, Mueller B, Lim K, Ugurbil K. Glutamate mapping at 3 and 4 Tesla in human brain using short TE proton echo planar spectroscopic imaging. In: Proceedings of the 13th Annual Meeting of ISMRM, Miami Beach, FL, USA, 2005 (Abstract 2515).
29. Provencher SW. Estimation of metabolite concentrations from localized in vivo proton NMR spectra. Magn Reson Med 1993;30:672–679.
30. Golman K, Ardenkjaer-Larsen JH, Petersson JS, Mansson S, Leunbach I. Molecular imaging with endogenous substances. Proc Natl Acad Sci USA 2003;100:10435–10439.
31. Dydak U, Weiger M, Pruessmann KP, Meier D, Boesiger P. Sensitivity-encoded spectroscopic imaging. Magn Reson Med 2001;46:713–722.
32. Dydak U, Pruessmann KP, Weiger M, Tsao J, Meier D, Boesiger P. Parallel spectroscopic imaging with spin-echo trains. Magn Reson Med 2003;50:196–200.
33. Guimaraes AR, Baker JR, Jenkins BG, Lee PL, Weisskoff RM, Rosen BR, Gonzalez RG. Echoplanar chemical shift imaging. Magn Reson Med 1999;41:877–882.
34. Griswold MA, Jakob PM, Heidemann RM, Nittka M, Jellus V, Wang J, Kiefer B, Haase A. Generalized autocalibrating partially parallel acquisitions (GRAPPA). Magn Reson Med 2002;47:1202–1210.
35. Wiggins GC, Triantafyllou C, Potthast A, Reykowski A, Nittka M, Wald LL. 32-channel 3 Tesla receive-only phased-array head coil with soccer-ball element geometry. Magn Reson Med 2006;56:216–223.